Shape and Dynamics of Adhesive Cells: Mechanical Response of Open Systems

Yuehua Yang and Hongyuan Jiang*
CAS Key Laboratory of Mechanical Behavior and Design of Materials, Department of Modern Mechanics, University of Science and Technology of China, Hefei, Anhui 230027, China
(Received 4 October 2016; published 19 May 2017)

Cell adhesion is an essential biological process. However, previous theoretical and experimental studies ignore a key variable, the changes of cellular volume and pressure, during the dynamic adhesion process. Here, we treat cells as open systems and propose a theoretical framework to investigate how the exchange of water and ions with the environment affects the shape and dynamics of cells adhered between two adhesive surfaces. We show that adherent cells can be either stable (convex or concave) or unstable (spontaneous rupture or collapse) depending on the adhesion energy density, the cell size, the separation of two adhesive surfaces, and the stiffness of the flexible surface. Strikingly, we find that the unstable states vanish when cellular volume and pressure are constant. We further show that the detachments of convex and concave cells are very different. The mechanical response of adherent cells is mainly determined by the competition between the loading rate and the regulation of the cellular volume and pressure. Finally, we show that as an open system the detachment of adherent cells is also significantly influenced by the loading history. Thus, our findings reveal a major difference between living cells and nonliving materials.

DOI: 10.1103/PhysRevLett.118.208102

Adhesion of cells to an extracellular matrix or another cell plays a fundamental role in many physiological processes, such as cell migration, wound healing, cell recognition, and rigidity sensing [1–5]. The adhesion strength and the rupture force are the key parameters to characterize cell adhesion. Consequently, the quantitative measurement of these properties of adhesive cells is essential for understanding the fundamental mechanisms of the adhesion-related processes and phenomena.

With the development of experimental techniques, such as micropipette aspiration [6–8], atomic force microscopy [9,10], optical tweezing [11], and microplate manipulation [12–16], the properties of cell adhesion and cell deformability have been extensively explored experimentally. Conventionally, the extraction of these properties from experimental data is mostly based on contact mechanics models [17,18], the Young-Dupré equation [6,19], or the model proposed by Brochard-Wyart and de Gennes [20–22]. In these models, cell volume is either assumed to be constant or totally ignored. However, when cells suffer from large deformation, cell volume, cortical tension, and hydrostatic pressure usually change dramatically [23–29] due to the extensive exchange of water and ions with the environment. For example, cell volume can increase by 30% during the mitotic cell rounding from the adherent state [25], and decrease by 30% under shear stress [26,27]. Cell volume can also change more than 40% due to osmotic shocks [28,29]. However, in such a nonequilibrium open system, how the shape and dynamics of adherent cells are affected by the cellular volume and pressure regulation is still elusive.

To answer this question, we focus on cells adhered symmetrically between two surfaces (Fig. 1) as frequently used in atomic force microscope, microplate manipulation, and micropipette aspiration experiments. One adhesive surface can be treated as a rigid body, and the other can be regarded as a cantilever with an equivalent spring stiffness [Fig. 1(c)]. First, the fixed end of the cantilever is moved downward d_0 to compress a spherical cell with an

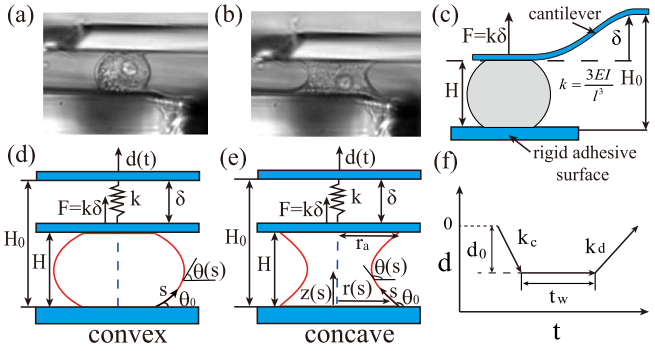

FIG. 1. Schematic of cells adhered symmetrically between an adhesive surface and a cantilever. Panels (a) and (b) show convex and concave cells observed in experiments (adapted from Ref. [15] with permission). (c) The deflection of the cantilever is $\delta = Fl^3/3EI$, where F is the force applied by the cell and EI is the bending stiffness of the cantilever. Thus, the cantilever can be treated as a spring with a stiffness of $k = 3EI/l^3$ and zero rest length. In (d) and (e), the cell shape is cylindrically symmetric and can be described by $r(s)$ and $z(s)$, where s is the arc length. $\theta(s)$ is the tangential angle of the arc length, and θ_0 is the contact angle. So the cell is convex when $\theta_0 < 90°$ and concave when $\theta_0 > 90°$. r_a is the adhesion radius. H is the cell height and H_0 is the separation of the adhesive surface and cantilever. $d(t)$ is the displacement of the fixed end of the cantilever. (f) The loading and unloading process.

initial radius of r_0 [Fig. 1(f)]. Then, we stop and hold the cantilever for a duration of t_w. After the waiting time t_w, the cell becomes either convex [Fig. 1(a)] or concave [Fig. 1(b)] due to adhesion, although the cell is always convex initially. Finally, the cantilever is moved upward at a speed k_d to induce detachment [Fig. 1(f)].

We treat cells as open systems, i.e., water and ions can pass through the cell membrane passively or actively. Therefore, the time evolution of the cellular volume V and the total number of ions n due to the transport of water and ions are [23]

$$\frac{dV}{dt} = -L_p A_{\mathrm{eff}}(\Delta P - \Delta\Pi), \tag{1}$$

$$\frac{dn}{dt} = A_{\mathrm{eff}}(J_{\mathrm{out}} + J_{\mathrm{in}}), \tag{2}$$

where A_{eff} is the effective surface area, i.e., the difference between the total surface area and the adhesion area. L_p is the membrane permeability rate to water. ΔP and $\Delta\Pi$ are the hydrostatic and osmotic pressure differences, respectively. J_{out} reflects the ion efflux due to the opening of passive mechanosensitive channels. J_{in} describes the influx of ions through ion pumps that actively pump ions into the cell. More details of the model are specified in the Supplemental Material [30].

The cell is surrounded by the cortical layer and cell membrane. Therefore, both the cortical tension T_{cortex} and membrane tension T_m contribute to the total surface tension T_s, i.e., $T_s = T_{\mathrm{cortex}} + T_m$ [63,64]. The cortical layer is modeled as a fluidlike layer with a constant active stress σ_a [65]. The stress in the cortical layer σ_{cortex} is described by $\sigma_{\mathrm{cortex}} = \eta\dot{\varepsilon}_A + \sigma_a$ [66], where $\dot{\varepsilon}_A$ is the strain rate of the cellular surface area and η is the viscosity of the cortical layer. Thus, the cortical tension is $T_{\mathrm{cortex}} = \sigma_{\mathrm{cortex}} h_c$, where h_c is the thickness of the cortical layer. The membrane tension is related to the membrane stress σ_m by $T_m = \sigma_m h_m$, where h_m is the membrane thickness. We can consider an equivalent surface stress σ in these two layers as $T_s = \sigma h$, where $h = h_m + h_c$. Therefore, the surface stress can be determined by $\sigma(h_m + h_c) = \sigma_{\mathrm{cortex}} h_c + \sigma_m h_m$. We can use a membrane reservoir model or a viscoelastic model to describe the membrane stress (see the Supplemental Material [30] for details), but we find the results of these two models are qualitatively the same (Figs. S3 and S5 of Ref. [30]). So we use the reservoir model for the simulations in the main text.

The force balance yields

$$2\pi\sigma h r \sin\theta = \Delta P \pi r^2 + F, \tag{3}$$

where θ is the tangential angle of the arc length, r is the cell radius, and F is the external force applied by the cantilever (Fig. 1). Notice that F is positive when the cell is stretched.

The contact angle θ_0 defined in Figs. 1(d) and 1(e) is given by the Young-Dupré equation as

$$\Gamma = \sigma h(1 - \cos\theta_0), \tag{4}$$

where Γ is the adhesion energy density between the cell and substrate. When $\Gamma = 0$, Eq. (4) is reduced to $\theta_0 = 0$, which is the situation discussed previously [23]. In general, Γ can vary with time due to the binding and unbinding of the ligand-receptor bonds. The time evolution of Γ is (see the Supplemental Material [30] for details)

$$\frac{d\Gamma}{dt} = \Gamma_0 k_{\mathrm{off}}^0 \left[1 - \frac{\Gamma}{\Gamma_0}\exp\left(\frac{aFV_e}{k_B T \Gamma \pi r_a^2}\right)\right], \tag{5}$$

where Γ_0 is the equilibrium adhesion energy density when $F = 0$, and k_{off}^0 is the dissociation rate of ligand-receptor pairs when $F = 0$. r_a is the adhesion radius, a is the characteristic length of the bond deformation, V_e is the rupture energy of a single bond [67], k_B is Boltzmann's constant, and T is the absolute temperature. Notice that at the steady state ($d\Gamma/dt = 0$), the equilibrium adhesion energy density Γ_s for nonzero F depends on the external force, i.e., $F = (k_B T \Gamma_s \pi r_a^2/aV_e)\ln(\Gamma_0/\Gamma_s)$.

First, we consider the dynamic adhesion with constant H_0 (the end of the cantilever is fixed). Here, we assume Γ_0 is very small (weak adhesion) and the waiting time t_w defined in Fig. 1(f) is long enough so that the cell has already reached the steady state. Then, we suddenly increase Γ_0 to find a new steady state. In this case, the contact angle θ_0 and adhesion radius r_a increase with time [Fig. 2(a), and Fig. S8 of Ref. [30]]. Meanwhile, the tip of the cantilever moves downward so that cell height H decreases and F increases until the cell reaches its new steady state.

For small Γ_0, we find the steady cell shape is convex ($\theta_0 < 90°$), but the cantilever can apply a pulling ($F > 0$) or pushing ($F < 0$) force [Fig. 2(a), and Movies S1 and S2 of Ref. [30]]. For large Γ_0, the cell undergoes a transition from a convex shape to a concave shape as $\Gamma(t)$ increases with time [light green curve in Fig. 2(a), subplot (II), and Movie S3 of Ref. [30]], and F changes from a pushing force to a pulling force. Therefore, there is a critical Γ_0, above which the steady adherent cell is concave ($\theta_0 > 90°$). Besides Γ_0, we find the separation between the two adhesive surfaces H_0 can also affect the steady cell shape. The cell is more likely to be concave for larger H_0, as shown in the phase diagram [Fig. 3(a)].

Interestingly, we find that the steady cell shape depends not only on Γ_0 and H_0, but also on the initial cell size r_0, i.e., the radius of the spherical cells in suspension. If we decrease r_0 from 18 μm [Fig. 3(a)] to 10.5 μm [Fig. 3(b)], another region appears in the phase diagram [dark green region in Fig. 3(b), and Movie S4 in Ref. [30]], where the "spontaneous rupture" of cells occurs due to the

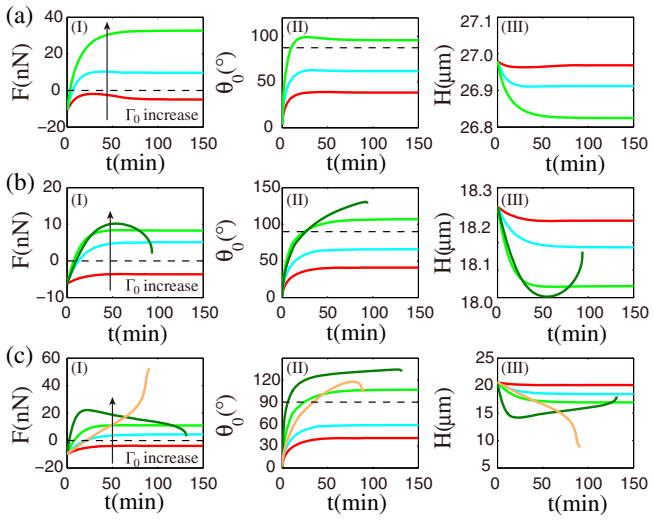

FIG. 2. Dynamic adhesion of cells adhered to an adhesive surface and a cantilever. (a) $r_0 = 18\ \mu$m, $k = 0.5$ N/m; (b) $r_0 = 10.5\ \mu$m, $k = 0.5$ N/m; (c) $r_0 = 10.5\ \mu$m, $k = 0.01$ N/m. The parameters H_0 and Γ_0 used here are marked by stars in Fig. 3. Other parameters are the same (Table S1 of Ref. [30]). The subplots show (I) external force F, (II) contact angle θ_0, and (III) cell height H. The red, light blue, and light green curves represent the dynamic process of reaching the three stable states: (1) the cell is convex ($\theta_0 < 90°$) and $F < 0$; (2) the cell is convex and $F > 0$; (3) the cell is concave ($\theta_0 > 90°$) and $F > 0$. The dark green and orange curves represent the spontaneous rupture and collapse of cells. The color of these curves corresponds to the color of the phase diagrams in Fig. 3. The dashed lines in subplots (I) and (II) indicate the lines of $F = 0$ and $\theta_0 = 90°$, respectively.

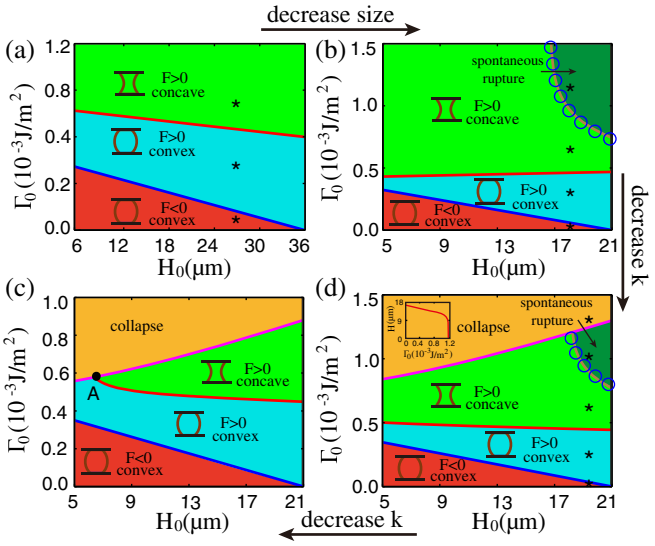

FIG. 3. Phase diagrams of cell shapes for various cantilever stiffnesses k and cell sizes r_0. (a) $r_0 = 18\ \mu$m, $k = 0.5$ N/m; (b) $r_0 = 10.5\ \mu$m, $k = 0.5$ N/m; (c) $r_0 = 10.5\ \mu$m, $k = 0.005$ N/m; (d) $r_0 = 10.5\ \mu$m, $k = 0.01$ N/m. There are three stable regions (red, light blue, and light green regions) and two unstable regions (dark green and orange regions). The stars indicate H_0 and Γ_0 used in Fig. 2. The blue circles in (b) and (d) are the theoretical predictions for the critical condition of the tension-induced rupture [30]. The inset in the orange region of (d) shows the collapse of the cell as Γ_0 increases.

adhesion-induced tension increases. The membrane tension increases rapidly and its time derivative is diverging at the time of rupture [dark green curves in Figs. S9(e) and S10(e) [30]]. In reality, when the tension is bigger than some critical value, the membrane and cortex will break. Here, because we did not consider the breakage of the membrane and cortex in the constitutive law, the membrane tension will keep increasing before cell rupture. This is similar to the rupture of red blood cells due to strong adhesion [68]. Mathematically, it indicates that for small cells there is a critical tension or cell height beyond which no catenoidlike solution exists [69]. The critical condition for the tension-induced rupture is given by Eq. (S48) in the Supplemental Material [30]. In this case, cell height H first decreases and then increases [dark green line in Fig. 2(b), subplot (III), and Movie S4 of Ref. [30]]. In contrast, F first increases and then decreases.

If the cantilever stiffness k decreases from 0.5 N/m [Fig. 3(b)] to 0.005 N/m [Fig. 3(c)], another region will emerge in the phase diagram [orange regions in Figs. 3(c) and 3(d), and Movie S5 of Ref. [30]]. In this case, the cell collapses to $H = 0$ when Γ_0 is large [inset in Fig. 3(d), orange region]. This is because under strong adhesion the cantilever is too soft to sustain the pulling force applied by the cell. Notably, the cell is easier to collapse for smaller H_0 [Figs. 3(c) and 3(d)]. Moreover, when k and H_0 are small enough, the cell may never become concave as Γ_0 increases. Instead, the cell will collapse at the convex stage [the left side of point A in Fig. 3(c)]. In fact, recent experiments found that when a cell spreads between a flexible microplate and a rigid microplate, the cell height can decrease to almost zero [15]. This is similar to but slightly different from the cell collapse we found here since the adhesion energy density used in the experiment is usually not very large and the occurrence of the full collapse may also be prevented by the resistance of cell organelles.

Strikingly, when cell volume is conserved during the spreading, the two unstable states (spontaneous rupture and collapse) vanish in the phase diagram (Fig. S11 [30]), and it is very hard for the cells to form a concave shape when k is small. Therefore, the regulation of cell volume and pressure directly induces the unique behaviors of spontaneous rupture and collapse we found here.

Now, we investigate the dynamic detachment of convex and concave cells. Here, we assume t_w is long enough so that the cell can reach the steady state after t_w (Fig. 1). Then, the fixed end of the cantilever is moved upward with a speed k_d to detach the cell. Here, we neglect the dynamics of Γ during detachment; i.e., Γ is constant, since we want to

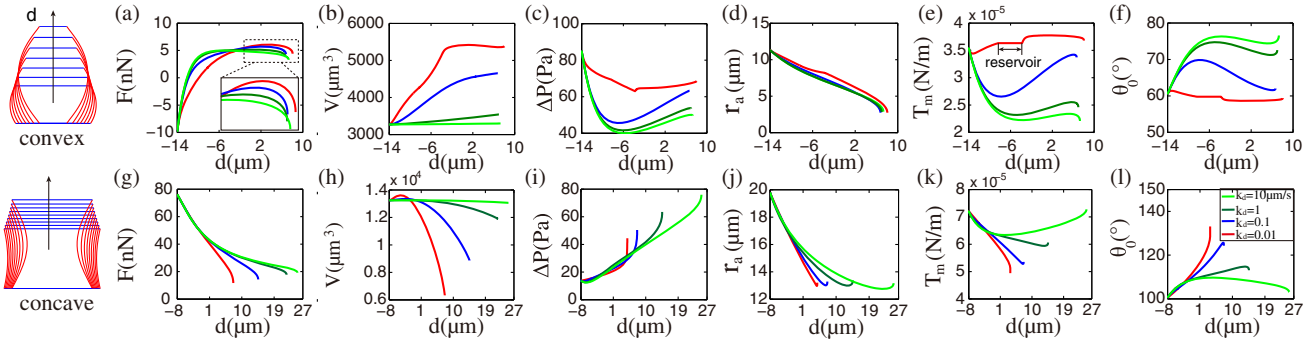

FIG. 4. Dynamic detachment of convex [(a)–(f)] and concave [(g)–(l)] cells that are initially at steady state; the initial compression is $d_0 = 14$ μm and $d_0 = 8$ μm for convex and concave cells, respectively. Left: the shape evolution during the detachment. The external force [(a),(g)], cellular volume [(b),(h)], hydrostatic pressure difference [(c),(i)], adhesion radius [(d),(j)], membrane tension [(e),(k)], and contact angle [(f),(l)] versus the displacement $d(t)$ with various loading speeds k_d.

focus on how cell volume regulation influences cell detachment. For convex cells, F first increases and then decreases slowly after reaching its maximum as the displacement d increases [Fig. 4(a)]. At steady state, there are two types of convex cells ($F < 0$ or $F > 0$). So F could be negative or positive initially. However, we find that the detachment processes of these two kinds of convex cells are qualitatively the same (Fig. S12 [30]). For concave cells, however, F is always positive and F decreases as d increases [Fig. 4(g)], which is very similar to the rupture of liquid bridges [70–73].

We find that the response of cells greatly depends on the loading rate k_d. If k_d is much larger than the speed of water and ion transport, the flux of water and ions is negligible and the cell volume is almost conserved [Figs. 4(b) and 4(h)]. In contrast, if k_d is comparable to or even smaller than the speed of water and ion transport, the change of cell volume is significant and it will greatly influence the hydrostatic pressure difference, membrane tension, and contact angle (Fig. 4). Interestingly, cell volume increases (cell swelling) for convex cells [Fig. 4(b)], while it decreases (cell shrinkage) for concave cells [Fig. 4(h)] during detachment. Furthermore, under small k_d, the membrane reservoir can be activated for convex cells [Fig. 4(e)], since the cell volume (surface area) increases remarkably. Thus, there are some windings on the curves of ΔP, T_m, and θ_0. Depending on the cell volume change and k_d, the membrane tension T_m could increase or decrease and it is not monotonic [Figs. 4(e) and 4(k)]. The change of θ_0 [Figs. 4(f) and 4(l)] is inverse to the change of T_m due to the constraint of the Young-Dupré equation [Eq. (4)]. Therefore, θ_0 is not constant, which indicates the assumption of constant θ_0 used previously [20] might be invalid if cells are treated as open systems.

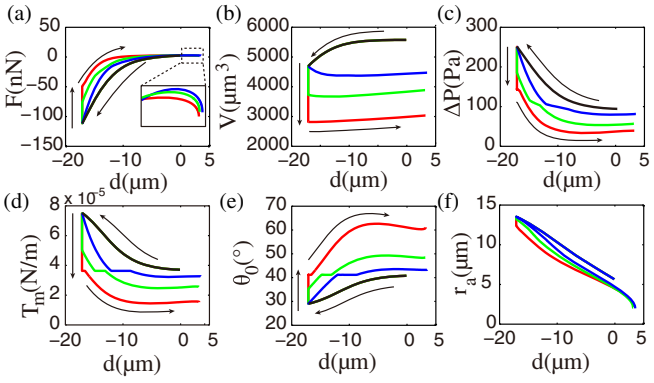

FIG. 5. The dynamic detachment of adhesive cells depends on loading history. The time evolution of the (a) external force, (b) cellular volume, (c) adhesion radius, (d) membrane tension, (e) contact angle, and (f) hydrostatic pressure difference of convex cells. For all the curves, $d_0 = 17$ μm, $k_c = k_d = 0.1$ μm/s, but the waiting time is different ($t_w = 0$, 400, and 800 s for the blue, green, and red curves). The black curves represent the loading stage.

For convex cells, the adhesion radius r_a first decreases steadily as d increases and then drops sharply when cell adhesion begins to rupture [Fig. 4(d)]. Conversely, for concave cells, r_a does not always decrease, but increases rapidly before the rupture [Fig. 4(j)]. This may be because convex cells rupture at the contact surfaces, while concave cells rupture at the necking equatorial section. These rupture forms are very similar to the rupture of liquid bridges [74].

Strikingly, our results for the dynamic spreading and detachment can quantitatively explain many existing experimental data (Fig. S13 [30]). Furthermore, we find the dynamic detachment of adherent cells also depends on loading history. To demonstrate it, we assume that the cell has already reached a steady state, and then we apply the loading-unloading process in Fig. 1(f) with various waiting times t_w. We find that the force, cell volume, contact angle, and other variables are very different (Fig. 5). This is because t_w is not long enough. Thus, the cell has not reached steady state before the cantilever is moved upward. In fact, the loading-unloading process in Fig. 1(f) is widely used in experiments [12–15], where the minimum t_w

needed to reach steady state can be affected by many factors, such as loading speed k_c, compression depth d_0, cell size, and cell type. Therefore, if t_w is not long enough, the mechanical response of cells in different experiments may not be comparable to each other.

In conclusion, we treated cells as open systems and studied how cell volume and pressure regulation influence the shape and dynamics of adherent cells. Our work showed that the mechanical response of living cells significantly depends on the complex interplay of cell volume change, loading rate, and loading history. Therefore, water and ion exchange with the environment is an essential factor that discriminates living cells from nonliving materials. Our findings may also have important implications for other biological processes accompanied by significant cell volume changes, such as mitotic cell rounding, cell deformation due to external forces, and haptotaxis or durotaxis induced by heterogeneous adhesion energy density or substrate stiffness.

This work was supported by the National Natural Science Foundation of China (Grants No. 11472271 and No. 11622222), the Thousand Young Talents Program of China, the Fundamental Research Funds for the Central Universities (Grant No. WK2480000001), and the Strategic Priority Research Program of the Chinese Academy of Sciences (Grant No. XDB22040403).

*Corresponding author.
jianghy@ustc.edu.cn

[1] H. F. Lodish, A. Berk, S. L. Zipursky, P. Matsudaira, D. Baltimore, J. Darnell *et al.*, Mol. Cell. Biol. **4** (2000).
[2] T. A. Springer *et al.*, Nature (London) **346**, 425 (1990).
[3] A. Elosegui-Artola, E. Bazellières, M. D. Allen *et al.*, Nat. Mater. **13**, 631 (2014).
[4] W. Engl, B. Arasi, L. Yap, J. Thiery, and V. Viasnoff, Nat. Cell Biol. **16**, 587 (2014).
[5] R. Mayor and S. Etienne-Manneville, Nat. Rev. Mol. Cell Biol. **17**, 97 (2016).
[6] E. Evans, D. Berk, and A. Leung, Biophys. J. **59**, 838 (1991).
[7] K. Prechtel, A. R. Bausch, V. Marchi-Artzner, M. Kantlehner, H. Kessler, and R. Merkel, Phys. Rev. Lett. **89**, 028101 (2002).
[8] B. Hogan, A. Babataheri, Y. Hwang, A. I. Barakat, and J. Husson, Biophys. J. **109**, 209 (2015).
[9] P.-H. Puech, K. Poole, D. Knebel, and D. J. Muller, Ultramicroscopy **106**, 637 (2006).
[10] S. Zou, H. Schonherr, and G. J. Vancso, J. Am. Chem. Soc. **127**, 11230 (2005).
[11] X. Liu, J. Q. Sun, M. H. Heggeness, M.-L. Yeh, and Z.-P. Luo, FEBS Lett. **563**, 23 (2004).
[12] O. Thoumine and J.-J. Meister, Eur. Biophys. J. **29**, 409 (2000).
[13] O. Thoumine and A. Ott, J. Cell Sci. **110**, 2109 (1997).
[14] N. Desprat, A. Richert, J. Simeon, and A. Asnacios, Biophys. J. **88**, 2224 (2005).
[15] D. Mitrossilis, J. Fouchard, D. Pereira, F. Postic, A. Richert, M. Saint-Jean, and A. Asnacios, Proc. Natl. Acad. Sci. U.S.A. **107**, 16518 (2010).
[16] O. Chaudhuri, S. H. Parekh, W. A. Lam, and D. A. Fletcher, Nat. Methods **6**, 383 (2009).
[17] V. T. Moy, Y. Jiao, T. Hillmann, H. Lehmann, and T. Sano, Biophys. J. **76**, 1632 (1999).
[18] Y.-S. Chu, S. Dufour, J. P. Thiery, E. Perez, and F. Pincet, Phys. Rev. Lett. **94**, 028102 (2005).
[19] M.-J. Colbert, A. Raegen, C. Fradin, and K. DalnokiVeress, Eur. Phys. J. E **30**, 117 (2009).
[20] F. Brochard-Wyart and P.-G. de Gennes, C.R. Phys. **4**, 281 (2003).
[21] S. Pierrat, F. Brochard-Wyart, and P. Nassoy, Biophys. J. **87**, 2855 (2004).
[22] M.-J. Colbert, F. Brochard-Wyart, C. Fradin, and K. Dalnoki-Veress, Biophys. J. **99**, 3555 (2010).
[23] H. Jiang and S. X. Sun, Biophys. J. **105**, 609 (2013).
[24] K. M. Stroka, H. Jiang, S.-H. Chen, Z. Tong, D. Wirtz, S. X. Sun, and K. Konstantopoulos, Cell **157**, 611 (2014).
[25] E. Zlotek-Zlotkiewicz, S. Monnier, G. Cappello, M. Le Berre, and M. Piel, J. Cell Sci. **211**, 765 (2015).
[26] J. Heo, F. Sachs, J. Wang, and S. Z. Hua, Cell. Physiol. Biochem. **30**, 395 (2012).
[27] I. Orhon *et al.*, Nat. Cell Biol. **18**, 657 (2016).
[28] M. P. Stewart, J. Helenius, Y. Toyoda, S. P. Ramanathan, D. J. Muller, and A. A. Hyman, Nature (London) **469**, 226 (2011).
[29] J. Irianto, J. Swift, R. P. Martins, G. D. McPhail, M. M. Knight, D. E. Discher, and D. A. Lee, Biophys. J. **104**, 759 (2013).
[30] See Supplemental Material at http://link.aps.org/supplemental/10.1103/PhysRevLett.118.208102, which includes Refs. [31–62], for more methods, discussions, figures, tables, and video files.
[31] M. Yoneda, J. Exp. Biol. **41**, 893 (1964).
[32] E. A. Evans, R. Skalak, and S. Weinbaum, *Mechanics and Thermodynamics of Biomembranes* (American Society of Mechanical Engineers, New York, 1980).
[33] E. Fischer-Friedrich, A. A. Hyman, F. Jülicher, D. J. Müller, and J. Helenius, Sci. Rep. **4**, 6213 (2015).
[34] S. Sukharev, B. Martinac, V. Y. Arshavsky, and C. Kung, Biophys. J. **65**, 177 (1993).
[35] D. Raucher and M. P. Sheetz, Biophys. J. **77**, 1992 (1999).
[36] L. Figard and A. M. Sokac, Bioarchitecture **4**, 39 (2014).
[37] B. Sinha, D. Koster, R. Ruez *et al.*, Cell **144**, 402 (2011).
[38] A. J. Kosmalska, L. Casares, A. Elosegui-Artola *et al.*, Nat. Commun., 7292 **6** (2015).
[39] R. Hochmuth and N. Mohandas, J. Biomech. **5**, 501 (1972).
[40] R. M. Hochmuth, N. Mohandas, and P. Blackshear Jr, Biophys. J. **13**, 747 (1973).
[41] E. A. Evans, Methods Enzymol. **173**, 3 (1989).
[42] L. Picas, F. Rico, and S. Scheuring, Biophys. J. **102**, L01 (2012).
[43] R. Rand, Biophys. J. **4**, 303 (1964).
[44] R. Hochmuth and R. Waugh, Annu. Rev. Physiol. **49**, 209 (1987).

[45] E. Evans and A. Yeung, Biophys. J. **56**, 151 (1989).
[46] A. R. Bausch, W. Möller, and E. Sackmann, Biophys. J. **76**, 573 (1999).
[47] E. J. Koay, A. C. Shieh, and K. A. Athanasiou, J. Biomech. Eng. **125**, 334 (2003).
[48] A. R. Bausch, F. Ziemann, A. A. Boulbitch, K. Jacobson, and E. Sackmann, Biophys. J. **75**, 2038 (1998).
[49] G. I. Bell *et al.*, Science **200**, 618 (1978).
[50] Y. Lin and L. B. Freund, Int. J. Solids Struct. **44**, 1927 (2007).
[51] J. Fouchard, C. Bimbard, N. Bufi, P. Durand-Smet, A. Proag, A. Richert, O. Cardoso, and A. Asnacios, Proc. Natl. Acad. Sci. U.S.A. **111**, 13075 (2014).
[52] H. Jiang, G. Huber, R. A. Pelcovits, and T. R. Powers, Phys. Rev. E **76**, 031908 (2007).
[53] H. Chen, T. Tang, and A. Amirfazli, Soft Matter **10**, 2503 (2014).
[54] T. R. Powers, G. Huber, and R. E. Goldstein, Phys. Rev. E **65**, 041901 (2002).
[55] M. P. Stewart, A. W. Hodel, A. Spielhofer, C. J. Cattin, D. J. Mller, and J. Helenius, Methods **60**, 186 (2013).
[56] K. D. Webster, W. P. Ng, and D. A. Fletcher, Biophys. J. **107**, 146 (2014).
[57] D. Mitrossilis, J. Fouchard, A. Guiroy, N. Desprat, N. Rodriguez, B. Fabry, and A. Asnacios, Proc. Natl. Acad. Sci. U.S.A. **106**, 18243 (2009).
[58] J. Y. Tinevez, U. Schulze, G. Salbreux, J. Roensch, J. F. Joanny, and E. Paluch, Proc. Natl. Acad. Sci. U.S.A. **106**, 18581 (2009).
[59] Mitra, K. I. Ubarretxena-Belandia, T. Taguchi, G. Warren, and D. M. Engelman, Proc. Natl. Acad. Sci. U.S.A. **101**, 4083 (2004).
[60] T. H. Hui, Z. L. Zhou, J. Qian, Y. Lin, A. H. W. Ngan, and H. Gao, Phys. Rev. Lett. **113**, 118101 (2014).
[61] E. H. Larsen, N. Møbjerg, and R. Nielsen, Comp. Biochm. Physiol., Part A, Mol. Integr. Physiol. **148**, 101 (2007).
[62] T. Erdmann and U. S. Schwarz, Phys. Rev. Lett. **92**, 108102 (2004).
[63] J. Dai and M. P. Sheetz, Biophys. J. **77**, 3363 (1999).
[64] A. Diz-Muñoz, D. A. Fletcher, and O. D. Weiner, Trends Cell Biol. **23**, 47 (2013).
[65] E. Fischer-Friedrich E, Y. Toyoda, C. J. Cattin, D. J. Müller, A. A. Hyman, and F. Jülicher, Biophys. J. **111**, 589 (2016).
[66] J. Tao and S. X. Sun, Biophys. J. **109**, 1541 (2015).
[67] L. Freund, Proc. Natl. Acad. Sci. U.S.A. **106**, 8818 (2009).
[68] A. Hategan, R. Law, S. Kahn, and D. E. Discher, Biophys. J. **85**: 2746 (2003).
[69] T. R. Powers, G. Huber, and R. E. Goldstein, Phys. Rev. E **65**, 041901 (2002).
[70] O. Pitois, P. Moucheront, and X. Chateau, Eur. Phys. J. B **23**, 79 (2001).
[71] O. Pitois, P. Moucheront, and X. Chateau, J. Colloid Interface Sci. **231**, 26 (2000).
[72] D. Rossetti, X. Pepin, and S. J. Simons, J. Colloid Interface Sci. **261**, 161 (2003).
[73] C. D. Willett, M. J. Adams, S. A. Johnson, and J. P. Seville, Langmuir **16**, 9396 (2000).
[74] A. Akbari and R. J. Hil, Soft Matter **12**, 6868 (2016).